

## On the Age Calibration of Open Clusters using Red Clump Stars

ABIGAIL R. CHRISS <sup>1</sup> AND GUY WORTHEY <sup>2</sup>

<sup>1</sup>*Department of Physics and Astronomy, Bowdoin College, 8800 College Station, Brunswick, ME 04011-8488, USA*

<sup>2</sup>*Department of Physics and Astronomy, Washington State University, 1245 Webster Hall, Pullman, WA 99164-2814, USA*

(Received February 28, 2024; Revised December 3, 2024; Accepted YYY)

### ABSTRACT

In this study, we extend the dust-independent [Hatzidimitriou \(1991\)](#) relation between cluster age and  $d_{B-R}$  color difference between the red giant branch (RGB) and red clump to younger cluster ages. We perform membership analysis on fourteen galactic open clusters using *Gaia* DR3 astrometry, then compute the difference in color of the RGB and red clump  $d_{B-R}$  using *Gaia* photometry. We also compute  $d_{B-R}$  for five fields surrounding Small Magellanic Cloud (SMC) clusters. We find that the trend derived from older clusters does not extrapolate to younger ages and becomes double-valued. We confirm that  $d_{B-R}$  is independent of metallicity. Current stellar evolutionary isochrones do not quantitatively reproduce the trend and furthermore predict an increased color gap with a decrease in metallicity that is not echoed in the data. Integrated light models based on current isochrones exaggerate the color change over the  $-0.5 < [\text{Fe}/\text{H}] < 0$  interval at the few-percent level.

*Keywords:* Open star clusters (1160) — Stellar ages (1581) — Red giant clump (1370) — Red giant branch (1368) — Hertzsprung Russell diagram (725)

### 1. INTRODUCTION

Star clusters represent both a crucial testing ground for the theory of stellar evolution and markers for the chemical and dynamical history of the Milky Way and other galaxies. While massive star clusters typically host multiple stellar populations ([Gratton et al. 2012](#)), lower-mass open clusters are currently presumed to be simple stellar populations (SSPs) of a single age and heavy element abundance pattern. Cluster ages are often derived from the color magnitude diagram (CMD), where, especially, the luminosity of the main sequence turnoff (MSTO) provides a theoretically robust chronometer ([Chaboyer 1995](#)).

Even assuming perfect comparison models, distance uncertainty and line of sight dust extinction add error to age estimates. [Hatzidimitriou \(1991\)](#), hereafter [H91](#), proposed a method that bypasses both dust and distance. The color of the He-burning red clump is subtracted from the color of the H-burning red giant branch (RGB) at the same luminosity. [H91](#) used Johnson-Cousins  $B$  and  $R$  filters and thus the color difference is  $d_{B-R}$ . Age was found to track  $d_{B-R}$  for clusters older than  $\sim 2$  Gyr and for a variety of heavy element abundances. A bonus advantage of this method is that red

clump stars are much brighter than MSTO stars, and thus the method could be applied to distant clusters.

The advent of star formation history reconstruction methods, where the entire CMD is fit with a swarm of stellar evolutionary isochrones ([Harris & Zaritsky 2001](#); [Dolphin 2002](#)), might explain why the [H91](#) formula has not seen wide use ([Girardi 2016](#)). [Girardi](#) notes, however, that the reconstructions for older ages rest upon red clump and RGB lifetimes, something predicted by stellar evolutionary theory only at the 20% level.

The purpose of the present work is to confirm and extend [H91](#)'s result. A red clump should exist in the CMD for ages as young as  $\sim 150$  Myr, corresponding to MSTO masses of  $\sim 5 M_{\odot}$ . We were curious if [H91](#)'s result extended to younger populations. To that end, we mined *Gaia* open cluster data for additional clusters with red clumps, with particular attention to clusters between 500 Myr and 2 Gyr in age.

We describe cluster membership discrimination and our derivation of isochrone-based ages in §2. The [H91](#) method is addressed in §3, and we discuss the result in §4.

### 2. CLUSTER SAMPLE AND MEMBERSHIP ANALYSIS

From open cluster lists (Kharchenko et al. 2013; Cantat-Gaudin et al. 2020) we selected clusters beyond the H91 list, initially in the age range 200 Myr to 2 Gyr. As the project developed, we added a few older clusters to test the repeatability of the H91 method. Ideal clusters lie nearby and bloom richly with stars.

For each of the fourteen galactic open clusters presented in Table 1 we performed a membership analysis before applying reddening corrections and analyzing the CMD. The probabilities of membership for stars in each cluster were estimated using position ( $\alpha, \delta$ ), proper motion ( $\mu_\alpha, \mu_\delta$ ), and parallax ( $\pi$ ) from *Gaia* Data Release 3 (DR3). Cluster centers, proper motion central locations, and parallaxes from SIMBAD served as a first guess for each cluster, though we allowed drifts from these values during the fitting process. For position and proper motion, we drew annuli around the central location and computed star density (number per square degree or number per km s<sup>-1</sup>, respectively) as a function of annulus bin radius ( $r$ ). We employed a least squares fitter to model functions for the total stars and the field star background. We modeled the cluster spatial profile as a Gaussian with a constant-density pedestal representing field stars (Figure 1). Based on position, for example, the cluster membership probability for each star  $i$  is

$$P_{\text{cluster}, (\alpha, \delta)}(i) = \frac{N_{\text{total}}(r_i) - N_{\text{field}}(r_i)}{N_{\text{total}}(r_i)},$$

where  $r_i$  is the distance of a star from the cluster center, and the number of counts per square degree  $N$  come from two (cluster and field) function fits to the density profile. In other words, the probability is the expected fraction of member stars as a function of distance from the cluster center.

The fit for proper motion assumed an exponential density profile for the cluster on top of a constant field density (Figure 2), the only difference being that the “distance” is the  $\Delta\mu$  from the cluster locus. The parallax distribution was fit with two Gaussians, a broad one for the field and a narrow one for the cluster (Figure 3). Cone search opening angles (column 7 in Table 1) were revisited if density profiles did not clearly reach an asymptote.

Given three separate probability estimates, the combined probability from separate  $P_{(\alpha, \delta)}$ ,  $P_\mu$ , and  $P_\pi$  estimates is computed as in Balaguer-Núñez et al. (1998), updated to include increased dimensionality as in Griggio & Bedin (2022). The resultant probability distribution for NGC 7789 is shown in Figure 4.

### 3. RESULTS

An example of a cleaned CMD appears in Figure 5 and the remainder of cluster CMDs appear in Appendix A.

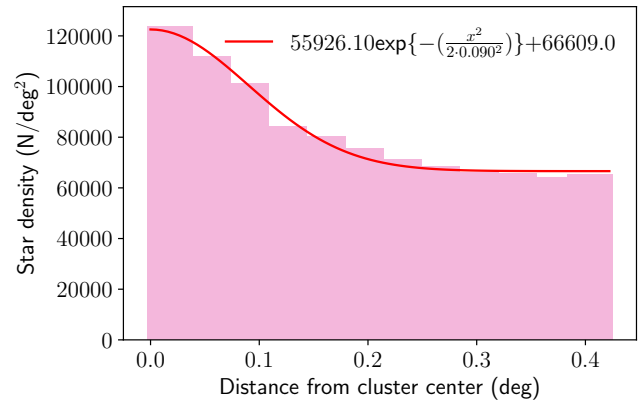


**Figure 1.** Stellar density in annuli proceeding from the center of the sky position of NGC 7789. A Gaussian model is shown (red). Field star density is taken as the constant-density asymptote.

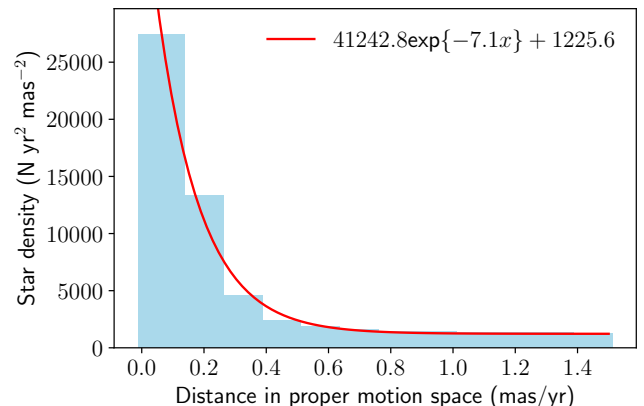


**Figure 2.** Stellar density in annuli proceeding from the center of the proper motion location of NGC 7789 amongst the field stars. An exponential model is shown (red). Field star density is taken as the constant-density asymptote.

From the CMDs we compute the central red clump color-magnitude location using the Tukey biweight statistic (Beers et al. 1990), which is similar to the median, in both  $BP - RP$  and  $G$ . The error in central location is estimated as  $\sigma = \sqrt{v/N}$ , where  $v$  is the biweight mid-variance and  $N$  is the number of red clump stars used for the calculation. RGB colors at the  $G$  magnitude of the red clump are found by overlaying the RGB segment of a PARSEC (Bressan et al. 2012) isochrone on the data, using synthetic photometry from the Worthey models to generate the  $BP - RP$  color. The synthetic RGB is then shifted left and right until fifty percent of stars were bluer and fifty percent of stars were redder. Once placed, the  $BP - RP$  magnitude at the  $G$  magnitude of the red clump is read from the shifted synthetic RGB. The clump stars outnumbered the RGB stars, so we ex-

**Table 1.** Age (log years) and errors from [Cantat-Gaudin et al. \(2020\)](#), color excess (magnitude) from [Kharchenko et al. \(2013\)](#), and color difference of red clump and RGB and errors (magnitude) for Milky Way open clusters in this study. Number of red clump stars with probability greater than 0.6 and opening angle for cone search (degrees) are also included. Metallicity from [Dias et al. \(2021\)](#) for Ruprecht 68 and NGC 2509, and from [Kharchenko et al. \(2013\)](#) for all other clusters.

Name	Age (log years)	$E(BP - RP)$ (mag)	[Fe/H] (dex)	$d_{BP-RP}$ (mag)	$N_{RC}(60)$	Opening angle (deg)
Melotte 71	$8.99 \pm 0.175$	0.139	-0.22	$0.118 \pm 0.035$	8	0.224
King 5	$9.01 \pm 0.175$	0.897	-0.30	$0.104 \pm 0.011$	8	0.272
NGC 2477	$9.05 \pm 0.175$	0.390	-0.192	$0.176 \pm 0.008$	58	0.450
NGC 1245	$9.08 \pm 0.175$	0.335	0.10	$0.107 \pm 0.008$	38	0.326
NGC 6208	$9.15 \pm 0.175$	0.279	-0.03	$0.082 \pm 0.009$	6	0.486
NGC 2509	$9.18 \pm 0.175$	0.139	0.082	$0.098 \pm 0.014$	3	0.179
NGC 7789	$9.19 \pm 0.175$	0.296	-0.24	$0.113 \pm 0.005$	35	0.422
NGC 2506	$9.22 \pm 0.175$	0.056	-0.20	$0.084 \pm 0.004$	33	0.263
NGC 2420	$9.24 \pm 0.175$	0.013	-0.38	$0.079 \pm 0.004$	7	0.210
Ruprecht 68	$9.26 \pm 0.15$	0.446	0.13	$0.151 \pm 0.022$	9	0.221
NGC 2627	$9.27 \pm 0.15$	0.139	-0.12	$0.066 \pm 0.010$	10	0.260
Melotte 66	$9.63 \pm 0.15$	0.167	-0.33	$0.123 \pm 0.006$	20	0.262
NGC 2682	$9.63 \pm 0.15$	0.067	-0.102	$0.103 \pm 0.004$	7	0.622
NGC 6791	$9.80 \pm 0.15$	0.157	0.32	$0.161 \pm 0.005$	36	0.204

**Table 2.** SMC fields in circular annuli centered around clusters, where the cluster names are given in column 1. The age (log years) from fits to PARSEC ([Bressan et al. 2012](#)) isochrones are applied to all fields, while the reddenings  $E(B - V)$  are applied separately to each. The radius of each cluster (degrees) from [Glatt et al. \(2010\)](#) is listed, and the aperture for field stars is an annulus from 1.5 times this radius to 5.0 times this radius. The number of red clump stars and the  $d_{BP-RP}$  color difference, transformed from  $d_{B-I}$ , are listed. A metallicity of  $[Fe/H] = -0.6$  ([Harris & Zaritsky 2004](#); [Idiart et al. 2007](#)) is assumed.

Name	Age (log years)	$E(B - V)$ (mag)	[Fe/H] (dex)	$d_{BP-RP}$ (mag)	N(RC)	Cluster radius (deg)
SMC 26		0.03		$0.160 \pm 0.005$	211	0.025
SMC 225		0.05		$0.168 \pm 0.011$	29	0.004
SMC 245		0.03		$0.122 \pm 0.008$	109	0.006
SMC 368		0.02		$0.148 \pm 0.009$	65	0.007
SMC 571		0.08		$0.145 \pm 0.005$	344	0.011
Average	$8.85 \pm 0.07$		-0.6	$0.148 \pm 0.004$		

pect counting statistics on the RGB to be the largest error source. We estimated RGB placement errors by shifting the theoretical RGB  $\pm$  one star from the median position, and taking the average of the absolute value of those two shifts.

Unsolved astrophysical effects and the placement of the initial red clump selection box may slightly skew the Tukey biweight for finding the central location. An example of an astrophysical effect occurs for clusters where the initial mass of a star at the RGB tip is  $\sim 2 M_{\odot}$ , of which our sample contains one example, NGC 7789. This cluster and NGC 752 ([Girardi et al. 2000](#)) have a clump with a few extra stars that are both lower luminosity and slightly blue. Significant spread in mass loss on the RGB combined with the fact that this mass might straddle the mass at which helium burning be-

gins in a degenerate versus a nondegenerate core might explain the effect. An example at older ages but high metallicity is NGC 6791, some of whose RGB stars may skip helium burning altogether ([Hansen 2005](#)).

Additional youthful clusters in the SMC were investigated using the Magellanic Clouds Photometric Survey ([Zaritsky et al. 2002](#)) but separation of cluster and field proved ambiguous. However, some the fields surrounding many of the clusters appeared to be amenable to analysis, with a large fraction of the stars appearing to land at a single, common age. We assumed a metallicity of  $[Fe/H] = -0.6$  ([Harris & Zaritsky 2004](#); [Idiart et al. 2007](#)) and fitted an age using PARSEC isochrones at an abundance value of  $[M/H] = -0.5$  as summarized in Table 2. Figure 6 illustrates CMDs for one of the five fields. The methods for calculating the

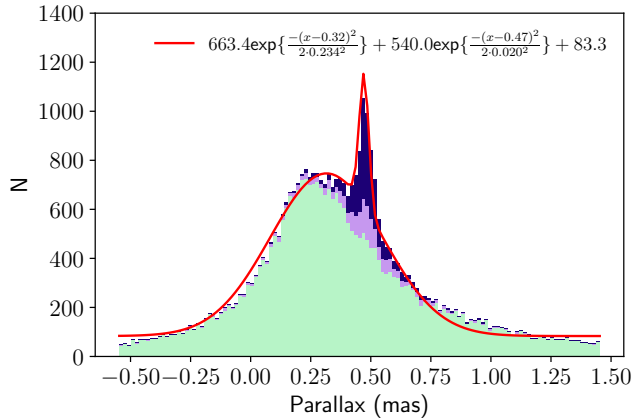


**Figure 3.** Distribution of stars in parallax in the NGC 7789 field. Stars nearest the proper motion locus (navy) and additional stars in a wider annulus (purple) form an obvious overdensity amongst the field stars (green). A two-Gaussian model is shown (red), with the broader component representing field stars.

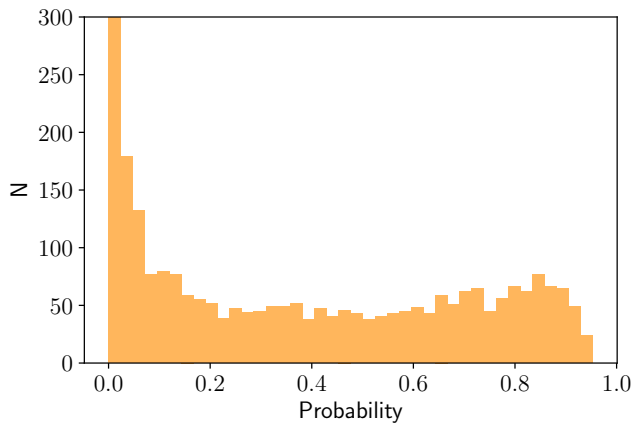


**Figure 4.** The resultant probability distribution after separate probabilities are combined for NGC 7789. The first bin contains about 20000 nonmember stars.

median location of the red clump and the RGB color at the level of the red clump are the same as those described above for the Milky Way clusters. For the SMC CMDs, we estimated the error in the RGB color as  $\delta = \sigma / \sqrt{N_{RGB}} = 0.2T_{RGB} / \sqrt{N_{RGB}}$ , where  $T_{RGB}$  is the thickness of the RGB at the level of the red clump and  $N_{RGB}$  is the number of RGB stars used to compute the median location. We estimated  $T_{RGB}$  as two times the color difference between the median and reddest RGB star. We assume that the spread in  $BP-RP$  of the RGB follows a normal distribution, so 99.38% of RGB stars at a given  $G$  magnitude are within 2.5 standard deviations of the median location. Thus  $2 \cdot 2.5\sigma = T_{RGB}$ .

For Milky Way clusters, we adopted ages and rough errors from Cantat-Gaudin et al. (2020), namely  $\pm 0.175$

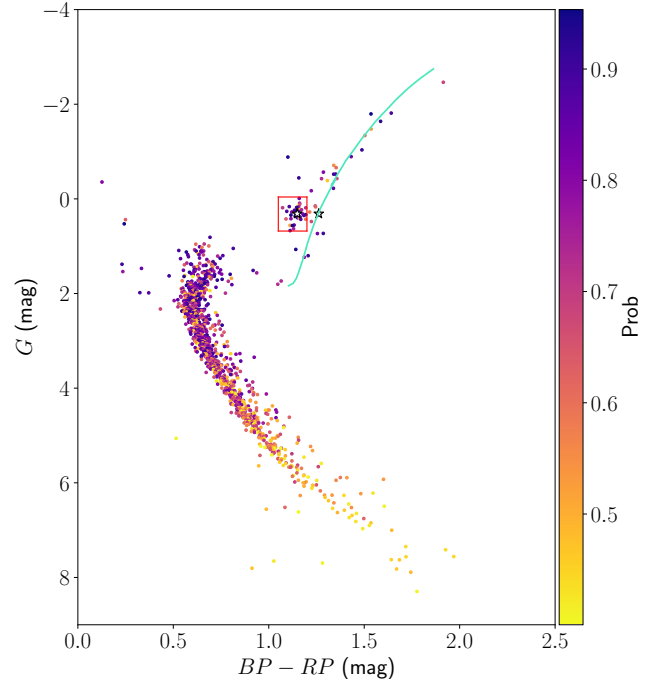


**Figure 5.** Color-absolute magnitude diagrams in *Gaia* passbands for probable members ( $P > 0.7$ ) of open cluster NGC 7789 using the distance and reddening from Table 1. Symbols are color mapped by membership probability as indicated by the color bar. A rectangle (red) indicating the estimated boundary of the red clump, along with the fitted RGB segment of a PARSEC isochrone at  $[\text{Fe}/\text{H}] = 0.00$  (turquoise), used to determine the median locations of the red clump and RGB are shown. The red clump and RGB loci are plotted as white stars with black outlines.

log years for clusters younger than 9.25 log years and  $\pm 0.15$  log years for older clusters. To plot H91’s data, we use ages and age error estimates from Kharchenko et al. (2013) for globular clusters Pal 12 and 47 Tuc and Beccari et al. (2012) for globular clusters Pal 4 and Eridanus. For SMC clusters, we use Da Costa & Hatzidimitriou (1998) and Mighell et al. (1998). For LMC clusters, we use Bomans et al. (1995) for NGC 1978, Kerber et al. (2007) for NGC 2173, Pieres et al. (2016) for Hodge 4 and ESO121-SC03, and Olszewski et al. (1991) for LW 47. We transform the H91 errors in age from years to log years using  $\delta(\log(t)) = \delta(t)/(t \ln 10)$ .

We took metallicities from Beccari et al. (2012) for Eridanus, Kharchenko et al. (2013) for Pal 12 and 47 Tuc, Harris (1996) for Pal 4, Kerber et al. (2007) for NGC 2173, and Pieres et al. (2016) for Hodge 4 and ESO121-SC03. For all other H91 clusters, we used the metallicity listed therein.

We used the algebraic formulae in Riello et al. (2021) to transform from the *Gaia* photometric system to Johnson-Cousins  $B - R$ . Color excess from Kharchenko

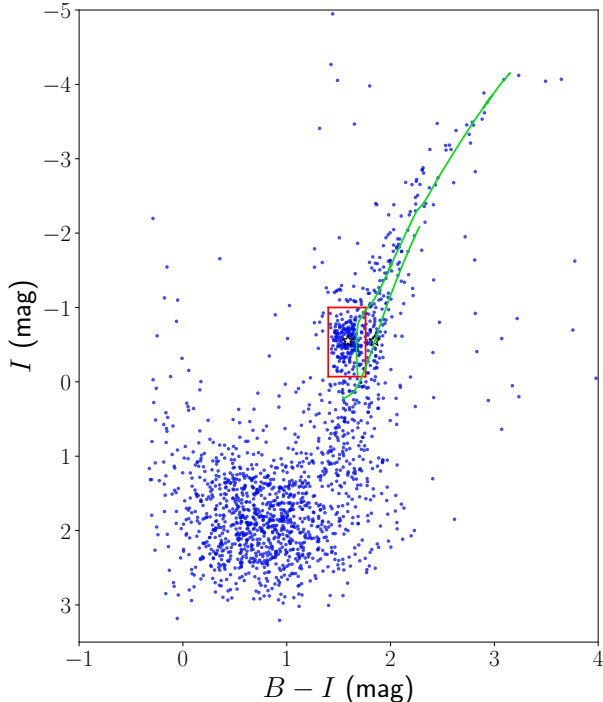


**Figure 6.** Color-absolute magnitude diagram of the field surrounding open cluster SMC 26, excluding the cluster itself. A rectangle (red) indicating the estimated boundary of the red clump, along with the fitted RGB segment a PARSEC isochrone at  $[M/H] = -0.5$  (green), used to determine the median locations of the red clump and RGB, are shown. The red clump and RGB loci are plotted as white stars with black outlines.

et al. (2013) was converted from  $E(B-V)$  to  $E(BP-RP)$  using Casagrande & Vandenberg (2018).

Results are summarized in Table 1 and shown in Figure 7 with the H91 fit, transformed to logarithmic age, overlaid.

#### 4. DISCUSSION AND CONCLUSION

From Figure 7 we find that the H91 line extrapolates poorly at the young end. At  $\log \text{age} = 9.25$ , or age = 1.8 Gyr, the two samples overlap in age, but every cluster in the new sample (this work) shows a wider  $d_{B-R}$  color separation. The magnitude of the effect exceeds any possible random or systematic uncertainties. The rise toward younger ages between  $\log \text{age} \sim 9.25$  and  $\sim 9.0$  means that going from  $d_{B-R}$  to age is double valued: One would need sufficient main sequence photometry to determine if the cluster was older or younger than  $\sim 2$  billion years before using either the old age H91 line or a young age line with a slope of opposite sign.

Even restricted to the new measurements, and further restricted to  $\log \text{age} < 9.5$ , the scatter appears to be astrophysical. A Kolmogorov-Smirnov test on our

$d_{BP-RP}$  values for clusters in our sample younger than  $9.5 \log \text{years}$  returned  $p \approx 1.62 \times 10^{-5}$ , indicating that the scatter is not drawn from a normal distribution. The cause of the scatter cannot be age, or we would see a slope in Figure 7. We sample metallicity span less well, but within that caveat, no metallicity dependence is evident. If neither age nor metallicity is the cause of the modulation in  $d_{B-R}$ , we are driven to consider more subtle causes such as variation in helium abundance, variation in the  $[\alpha/Fe]$  ratio, or variation in binary separation distributions. The investigation into the cause of the scatter must await future work.

We examine some predictions from stellar evolution theory in Figure 8. All isochrones were translated from  $T_{\text{eff}}$  and  $\log L$  to  $B-R$  using the empirical transformations of Worthey & Lee (2011). We show BaSTI 5.0.1 (Pietrinferni et al. 2004), BaSTI updated (Hidalgo et al. 2018), Padova, retrieved 2011 (Marigo et al. 2008), at two abundance values, and PARSEC+COLIBRI (Bresnan et al. 2012; Pastorelli et al. 2020) with Riemers (Reimers 1977)  $\eta = 0.2$ , retrieved 2023, also at two abundance values. Within the isochrone files, red clumps were located by treating the isochrone as a stellar population, predicting relative numbers of stars, and choosing the dominant sampling point to correspond to the red clump location. On the positive side, all evolutionary sets are within  $\sim 0.1 \text{ mag}$  (about 150 K) of the observed color delta, and all sets show a growth in  $d_{B-R}$  for ancient stellar populations that qualitatively mimics the observations.

If precision better than 150 K are desired, theory does not match observation. In particular, reading from Figure 8, theory predicts a metallicity dependence of roughly  $\frac{d(B-R)}{d[Fe/H]} \geq -0.2 \text{ mag per decade}$  in heavy element abundance. A metallicity dependence this large is strictly ruled out by the data, which includes clusters from the large and small Magellanic Clouds. For example, super-metal-rich cluster NGC 6791 lies right among SMC clusters. The presence of this systematic among current isochrone sets affects CMD decompositions (Harris & Zaritsky 2001; Dolphin 2002). It also impacts integrated light models by introducing a fictitious color drift in the sense to make metal rich populations redder.

To estimate the size of the induced integrated light color change, we employ evolutionary population synthesis models (Worthey et al. 2022). As of this writing, these models have eight options for stellar evolution, but the earliest one (Worthey 1994) uses the H91 scheme to place the red clump. We added an extra line of code to add a temperature shift, and translated the models that span metallicity in Figure 8 from  $\Delta \text{color}$  to  $\Delta \text{tempera-}$

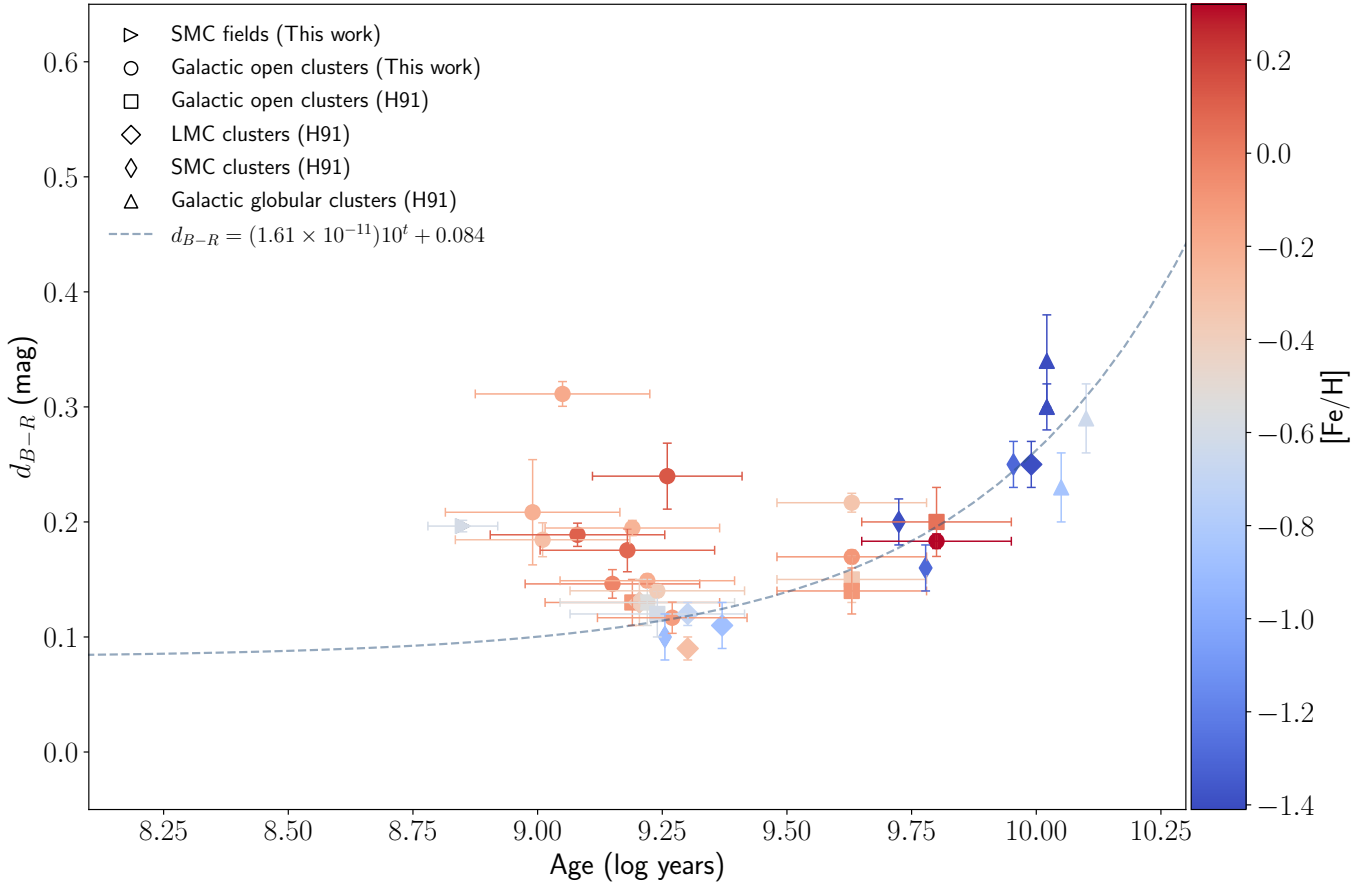


**Figure 7.** Color delta versus log age for galactic open clusters (circles) and average of SMC fields (right-facing triangles) from this work, along with globular clusters (squares), SMC clusters (thin diamonds), and LMC clusters (wide diamonds) from H91 color mapped by metallicity as indicated by the color bar. The H91 linear fit (dashed line) is also shown.

ture via Worthey & Lee (2011). The results are summarized in Table 3. Because the main sequence dominates in the blue,  $U - V$  is affected very little, but there is about a 4% effect in  $V - K$ .

Modelers should be aware of this discrepancy between current stellar evolution theory and observation because it adds to a list of ill-modeled or un-modeled effects that are far larger than the RMS fit between galaxy spectra and model integrated light spectra. Conroy et al. (2014), for example, find fits as good as 0.2% RMS, but their red clump temperatures do not adhere to H91 and so could be off by several percent. Blue stragglers are not included, which can lead to errors of over a magnitude in the terrestrial UV (Deng et al. 1999). Chemically peculiar stars, not included, alter the blue spectrum by  $\sim 2\%$  in the blue (Worthey & Shi 2023). Binary evolution products, carbon stars, and metallicity-composite populations are likewise not modeled, and yet the optical spectrum matches to 0.2%. The reason the fit is excellent is a generalization the age-metallicity degeneracy (Worthey 1994), where instead of age or metallicity, one

**Table 3.** Integrated light systematic color error if theoretical  $Z$  dependence is allowed to flourish.

Quantity	log age = 9	log age = 9.5	log age = 10
$\Delta T_{\text{eff}}$	172 K	93 K	212 K
$U - V$ , MP, H91	0.75	1.11	1.43
$U - V$ , MR, H91	1.04	1.58	1.99
$U - V$ , MR, $+\Delta\text{theory}$	1.04	1.58	1.99
Excess $U - V$	0.004	0.002	0.003
$V - K$ , MP, H91	2.39	2.73	3.04
$V - K$ , MR, H91	2.70	3.33	3.81
$V - K$ , MR, $+\Delta\text{theory}$	2.74	3.35	3.85
Excess $V - K$	0.038	0.021	0.037

inserts the concept of stellar temperatures in general. While some astrophysical inferences, such as abundance ratios, are somewhat isolated from this degeneracy, others, such as age, metallicity, age spread, or metallicity spread are not.

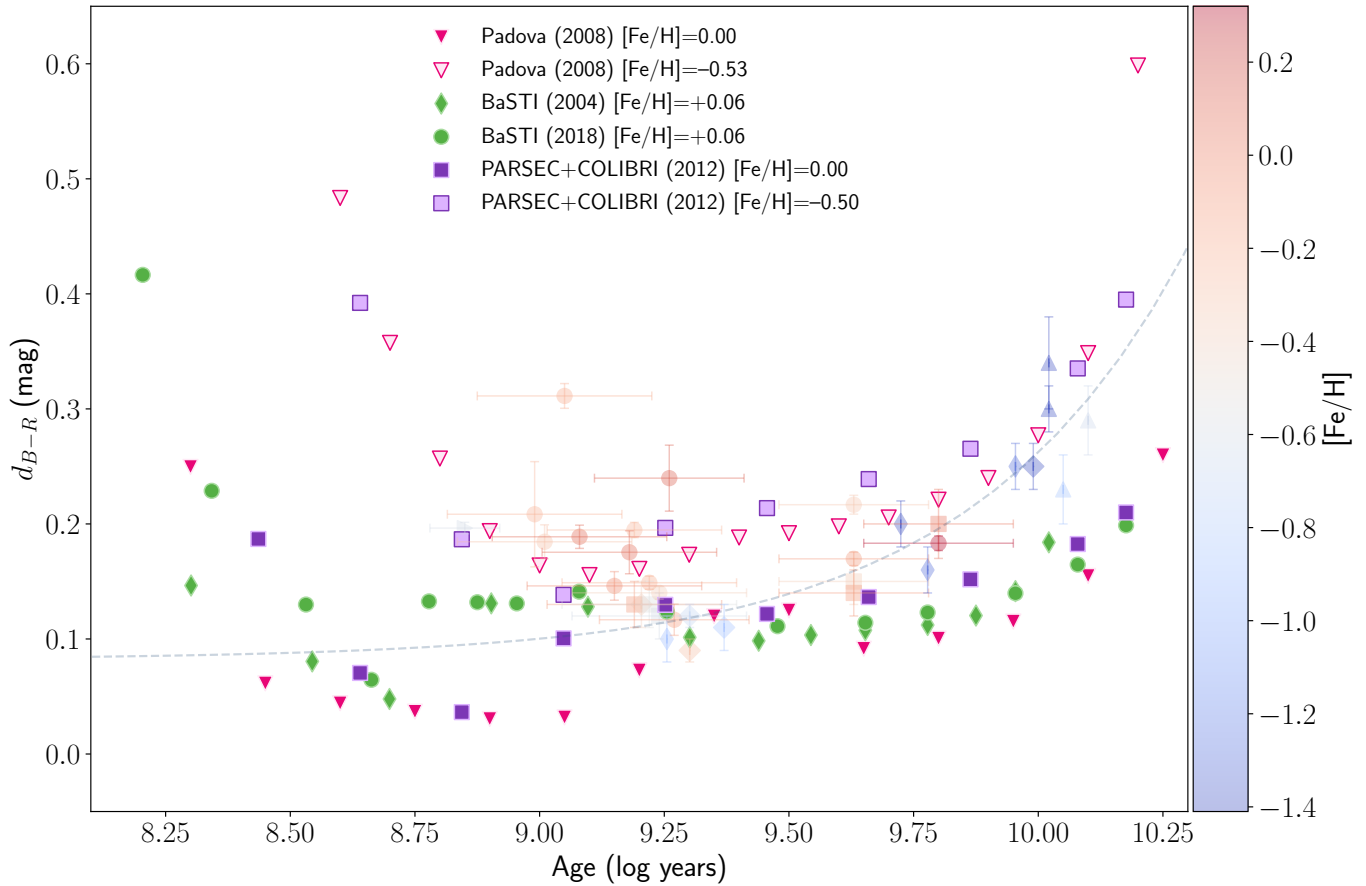


**Figure 8.** Color delta versus log age. Symbols are the same as Figure 7 with the addition of predictions from various isochrone sets: We show (Marigo et al. 2008) at two abundance values (pink triangles, unfilled for the metal poor sequence), BaSTI 5.0.1 (Pietrinferni et al. 2004) (green diamonds), BaSTI (Hidalgo et al. 2018) (green circles), and PARSEC+COLIBRI (Bressan et al. 2012; Pastorelli et al. 2020) at two abundance values (purple squares, unfilled for the metal poor sequence).

Future work on red clump systematics might include cross matching *Gaia*’s star list with photometric catalogs with accuracies better than *Gaia*’s  $BP - RP$ . The costs might include possible loss of stars from the sample and also possible exposure to systematic error caused by transforming from heterogeneous photometric systems to a common one. To target more clusters might also be contemplated, but the key is to cover parameter space, and the present combined data of H91 and ourselves covers well what the Milky Way provides.

We checked Milky Way clusters in this study that were also included in the PanSTARRS catalog to see if PanSTARRS photometry would clarify the CMDs and increase the accuracy of red clump or RGB color measurement. We cross matched *Gaia* and PanSTARRS photometry for stars with *Gaia*-estimated membership probability greater than 20% and brighter than  $G = 16$  mag. However, we found no improvement in red clump and RGB statistics. An example is shown in Figure 9.

There are young-age limits for the  $d_{B-R}$  method. For ages less than  $\sim 150$  Myr (log age 8.2), or, equivalently,

MSTO masses greater than  $\sim 5 M_{\odot}$ , stellar evolution through the RGB tip sparks no helium flash, and the helium-burning “blue plumes” no longer resemble red clumps. But there is a softer, practical limit that sets in around 600 Myr (log age 8.8) in which the RGB tip becomes fainter with youth, nearing the red clump luminosity. This decreases the number of first-ascent giants available for counting and increases uncertainty.

#### ACKNOWLEDGEMENTS

A.C. gratefully acknowledges the support of the Research Experiences for Undergraduates program, sponsored by the National Science Foundation Division of Physics Grant #2050866. The WSU Department of Physics and Astronomy provided additional support. This work has made use of data from the European Space Agency (ESA) mission *Gaia* (<https://www.cosmos.esa.int/gaia>), processed by the *Gaia* Data Processing and Analysis Consortium (DPAC, <https://www.cosmos.esa.int/web/gaia/dpac/consortium>). Funding for the DPAC has been provided by national institu-

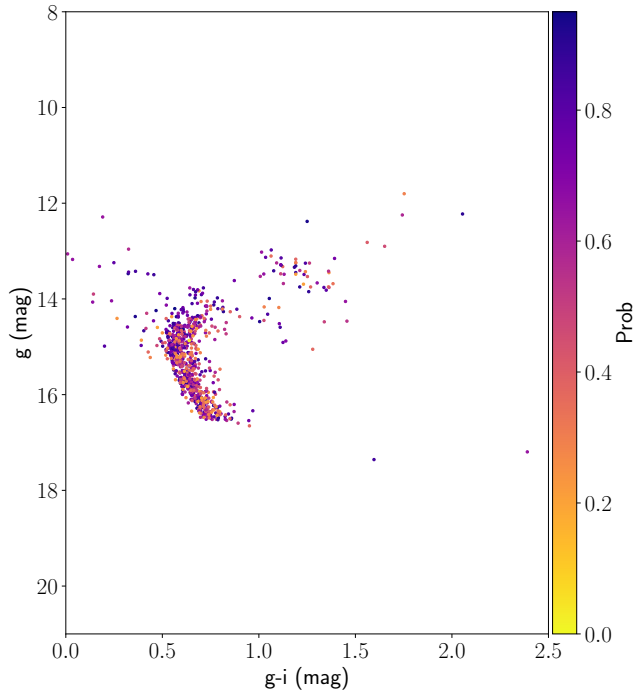


**Figure 9.** Color-apparent magnitude diagram of NGC 7789 from PanSTARRS  $g$  and  $i$  passbands. Points are colored by *Gaia* membership probability as indicated by the color bar. Stars with apparent *Gaia*  $G$  magnitudes greater than 16 mag were not included in the cross-match so are not plotted.

tions, in particular the institutions participating in the *Gaia* Multilateral Agreement. This research also made use of the SIMBAD database, operated at CDS, Strasbourg, France.

*Software:* Astropy (Astropy Collaboration et al. 2013, 2018, 2022), SciPy (Virtanen et al. 2020)

## APPENDIX

### A. COLOR MAGNITUDE DIAGRAMS

The CMDs of all fourteen Milky Way open clusters and five SMC fields used in this work are presented here. For each figure, we zoom in on the RGB and include the estimated boundary of the red clump, the fitted RGB segment of a solar-metallicity PARSEC isochrone, and the red clump and RGB loci to illustrate the method.

## REFERENCES

- Astropy Collaboration, Robitaille, T. P., Tollerud, E. J., et al. 2013, *A&A*, 558, A33, doi: [10.1051/0004-6361/201322068](https://doi.org/10.1051/0004-6361/201322068)
- Astropy Collaboration, Price-Whelan, A. M., Sipőcz, B. M., et al. 2018, *AJ*, 156, 123, doi: [10.3847/1538-3881/aabc4f](https://doi.org/10.3847/1538-3881/aabc4f)
- Astropy Collaboration, Price-Whelan, A. M., Lim, P. L., et al. 2022, *ApJ*, 935, 167, doi: [10.3847/1538-4357/ac7c74](https://doi.org/10.3847/1538-4357/ac7c74)
- Balaguer-Núñez, L., Tian, K. P., & Zhao, J. L. 1998, *A&AS*, 133, 387, doi: [10.1051/aas:1998324](https://doi.org/10.1051/aas:1998324)
- Beccari, G., Lützgendorf, N., Olczak, C., et al. 2012, *ApJ*, 754, 108, doi: [10.1088/0004-637X/754/2/108](https://doi.org/10.1088/0004-637X/754/2/108)
- Beers, T. C., Flynn, K., & Gebhardt, K. 1990, *AJ*, 100, 32, doi: [10.1086/115487](https://doi.org/10.1086/115487)
- Bomans, D. J., Vallenari, A., & de Boer, K. S. 1995, *A&A*, 298, 427
- Bressan, A., Marigo, P., Girardi, L., et al. 2012, *MNRAS*, 427, 127, doi: [10.1111/j.1365-2966.2012.21948.x](https://doi.org/10.1111/j.1365-2966.2012.21948.x)
- Cantat-Gaudin, T., Anders, F., Castro-Ginard, A., et al. 2020, *A&A*, 640, A1, doi: [10.1051/0004-6361/202038192](https://doi.org/10.1051/0004-6361/202038192)
- Casagrande, L., & Vandenberg, D. A. 2018, *MNRAS*, 479, L102, doi: [10.1093/mnras/sly104](https://doi.org/10.1093/mnras/sly104)
- Chaboyer, B. 1995, *ApJL*, 444, L9, doi: [10.1086/187847](https://doi.org/10.1086/187847)
- Conroy, C., Graves, G. J., & van Dokkum, P. G. 2014, *ApJ*, 780, 33, doi: [10.1088/0004-637X/780/1/33](https://doi.org/10.1088/0004-637X/780/1/33)
- Da Costa, G. S., & Hatzidimitriou, D. 1998, *AJ*, 115, 1934, doi: [10.1086/300340](https://doi.org/10.1086/300340)



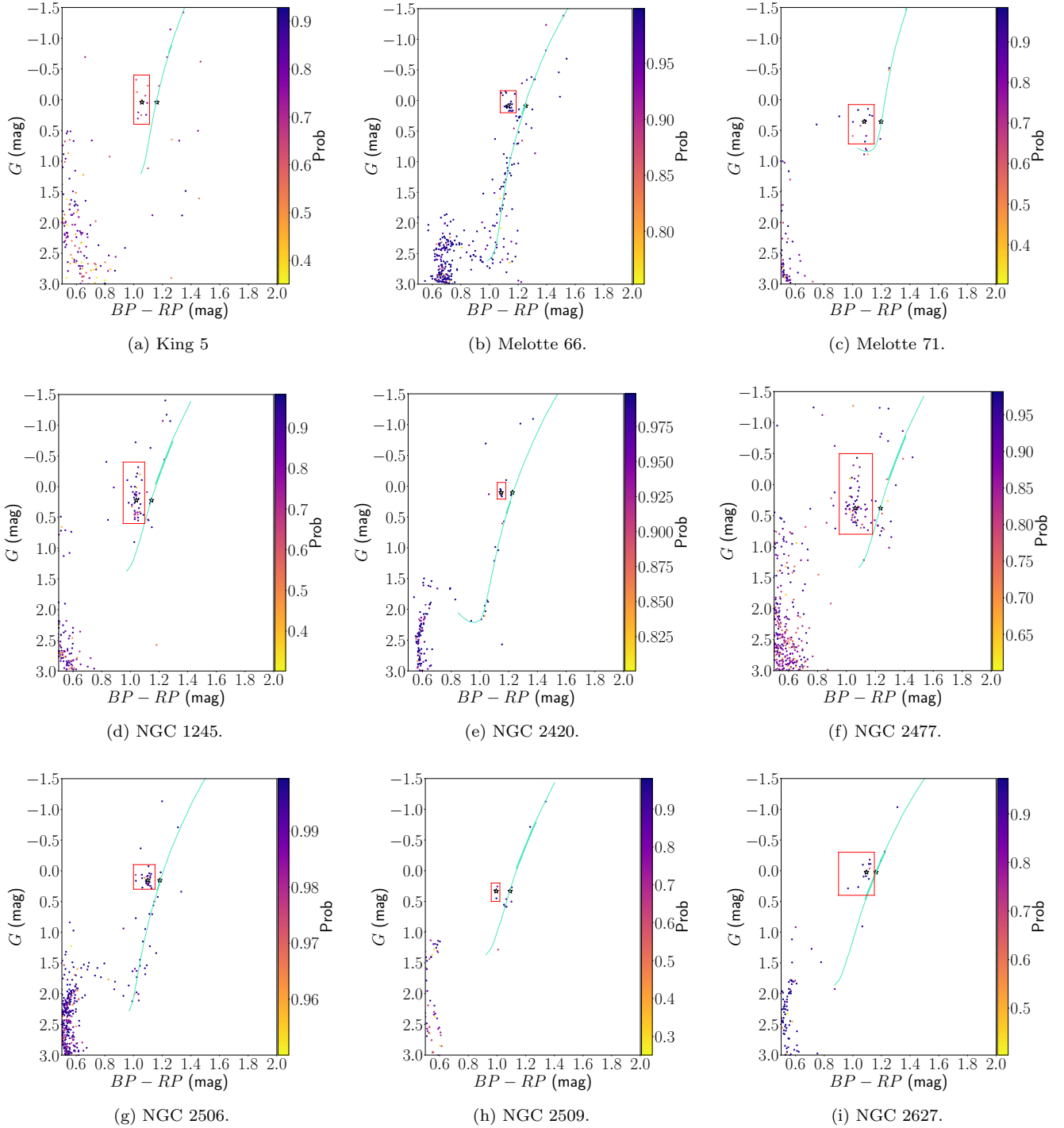


**Figure 10.** Color-absolute magnitude diagrams in *Gaia* passbands for probable members of several Milky Way open clusters using the distance and reddening from Table 1. Symbols and colors are the same as in Figure 5.

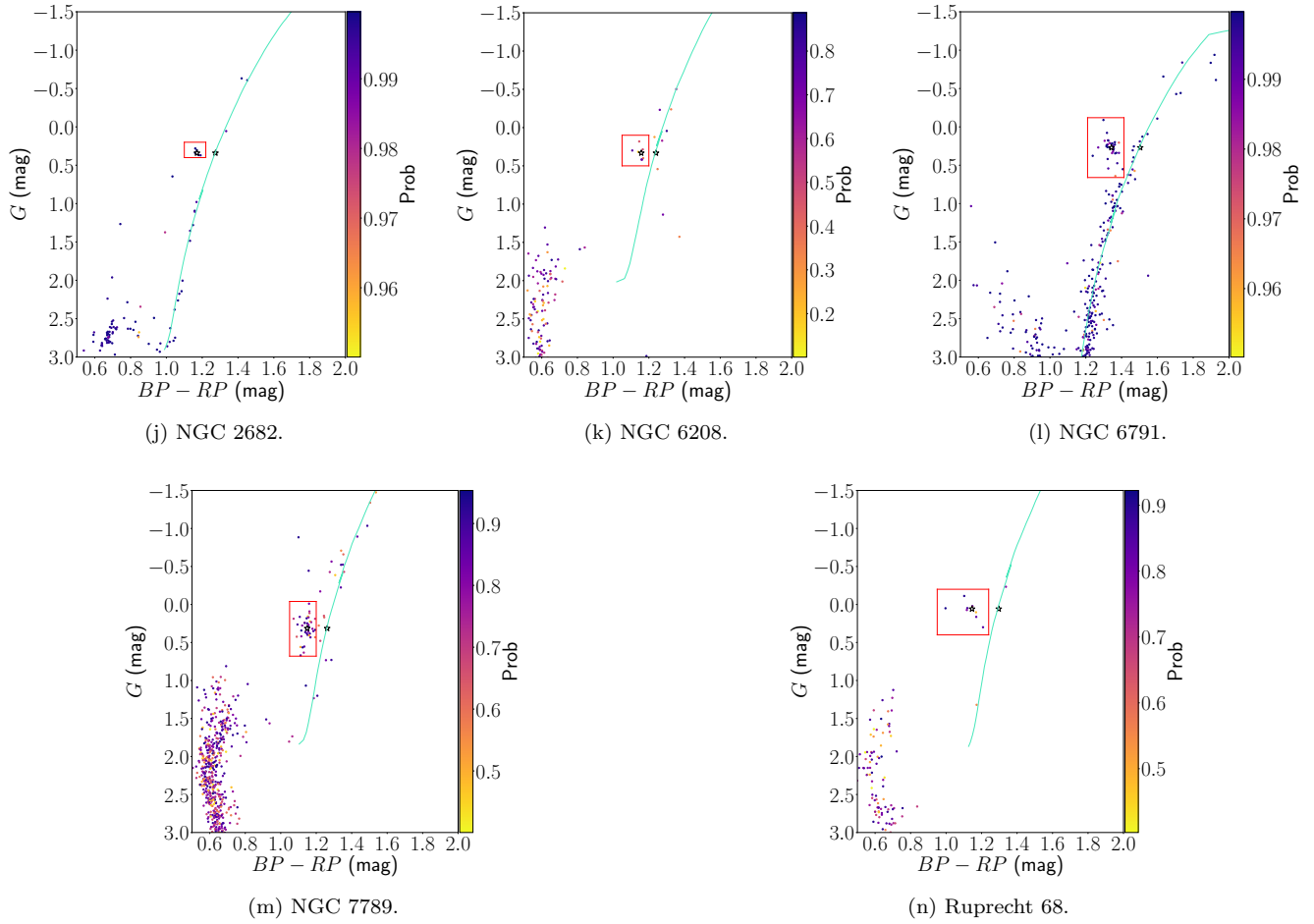


**Figure 11.** CMDs of galactic open clusters continued from Figure 10.

- Deng, L., Chen, R., Liu, X. S., & Chen, J. S. 1999, *ApJ*, 524, 824, doi: [10.1086/307832](https://doi.org/10.1086/307832)
- Dias, W. S., Monteiro, H., Moitinho, A., et al. 2021, *MNRAS*, 504, 356, doi: [10.1093/mnras/stab770](https://doi.org/10.1093/mnras/stab770)
- Dolphin, A. E. 2002, *MNRAS*, 332, 91, doi: [10.1046/j.1365-8711.2002.05271.x](https://doi.org/10.1046/j.1365-8711.2002.05271.x)
- Girardi, L. 2016, *ARA&A*, 54, 95, doi: [10.1146/annurev-astro-081915-023354](https://doi.org/10.1146/annurev-astro-081915-023354)
- Girardi, L., Mermilliod, J. C., & Carraro, G. 2000, *A&A*, 354, 892, doi: [10.48550/arXiv.astro-ph/0001068](https://doi.org/10.48550/arXiv.astro-ph/0001068)
- Glatt, K., Grebel, E. K., & Koch, A. 2010, *A&A*, 517, A50, doi: [10.1051/0004-6361/201014187](https://doi.org/10.1051/0004-6361/201014187)
- Gratton, R. G., Carretta, E., & Bragaglia, A. 2012, *A&A Rv*, 20, 50, doi: [10.1007/s00159-012-0050-3](https://doi.org/10.1007/s00159-012-0050-3)
- Griggio, M., & Bedin, L. R. 2022, *MNRAS*, 511, 4702, doi: [10.1093/mnras/stac391](https://doi.org/10.1093/mnras/stac391)
- Hansen, B. M. S. 2005, *ApJ*, 635, 522, doi: [10.1086/496951](https://doi.org/10.1086/496951)
- Harris, J., & Zaritsky, D. 2001, *ApJS*, 136, 25, doi: [10.1086/321792](https://doi.org/10.1086/321792)
- . 2004, *AJ*, 127, 1531, doi: [10.1086/381953](https://doi.org/10.1086/381953)
- Harris, W. E. 1996, *AJ*, 112, 1487, doi: [10.1086/118116](https://doi.org/10.1086/118116)
- Hatzidimitriou, D. 1991, *MNRAS*, 251, 545, doi: [10.1093/mnras/251.4.545](https://doi.org/10.1093/mnras/251.4.545)
- Hidalgo, S. L., Pietrinferni, A., Cassisi, S., et al. 2018, *ApJ*, 856, 125, doi: [10.3847/1538-4357/aab158](https://doi.org/10.3847/1538-4357/aab158)
- Idiart, T. P., Maciel, W. J., & Costa, R. D. D. 2007, *A&A*, 472, 101, doi: [10.1051/0004-6361:20077674](https://doi.org/10.1051/0004-6361:20077674)
- Kerber, L. O., Santiago, B. X., & Brocato, E. 2007, *A&A*, 462, 139, doi: [10.1051/0004-6361:20066128](https://doi.org/10.1051/0004-6361:20066128)
- Kharchenko, N. V., Piskunov, A. E., Schilbach, E., Röser, S., & Scholz, R. D. 2013, *A&A*, 558, A53, doi: [10.1051/0004-6361/201322302](https://doi.org/10.1051/0004-6361/201322302)
- Marigo, P., Girardi, L., Bressan, A., et al. 2008, *A&A*, 482, 883, doi: [10.1051/0004-6361:20078467](https://doi.org/10.1051/0004-6361:20078467)
- Mighell, K. J., Sarajedini, A., & French, R. S. 1998, *AJ*, 116, 2395, doi: [10.1086/300591](https://doi.org/10.1086/300591)
- Olszewski, E. W., Schommer, R. A., Suntzeff, N. B., & Harris, H. C. 1991, *AJ*, 101, 515, doi: [10.1086/115701](https://doi.org/10.1086/115701)
- Pastorelli, G., Marigo, P., Girardi, L., et al. 2020, *MNRAS*, 498, 3283, doi: [10.1093/mnras/staa2565](https://doi.org/10.1093/mnras/staa2565)
- Pieres, A., Santiago, B., Balbinot, E., et al. 2016, *Monthly Notices of the Royal Astronomical Society*, 461, 519, doi: [10.1093/mnras/stw1260](https://doi.org/10.1093/mnras/stw1260)
- Pietrinferni, A., Cassisi, S., Salaris, M., & Castelli, F. 2004, *ApJ*, 612, 168, doi: [10.1086/422498](https://doi.org/10.1086/422498)
- Reimers, D. 1977, *A&A*, 61, 217
- Riello, M., De Angeli, F., Evans, D. W., et al. 2021, *A&A*, 649, A3, doi: [10.1051/0004-6361/202039587](https://doi.org/10.1051/0004-6361/202039587)
- Virtanen, P., Gommers, R., Oliphant, T. E., et al. 2020, *Nature Methods*, 17, 261, doi: [10.1038/s41592-019-0686-2](https://doi.org/10.1038/s41592-019-0686-2)
- Worthey, G. 1994, *ApJS*, 95, 107, doi: [10.1086/192096](https://doi.org/10.1086/192096)
- Worthey, G., & Lee, H.-c. 2011, *ApJS*, 193, 1, doi: [10.1088/0067-0049/193/1/1](https://doi.org/10.1088/0067-0049/193/1/1)
- Worthey, G., & Shi, X. 2023, *MNRAS*, 518, 4106, doi: [10.1093/mnras/stac3297](https://doi.org/10.1093/mnras/stac3297)
- Worthey, G., Shi, X., Pal, T., Lee, H.-c., & Tang, B. 2022, *MNRAS*, 511, 3198, doi: [10.1093/mnras/stac267](https://doi.org/10.1093/mnras/stac267)
- Zaritsky, D., Harris, J., Thompson, I. B., Grebel, E. K., & Massey, P. 2002, *AJ*, 123, 855, doi: [10.1086/338437](https://doi.org/10.1086/338437)

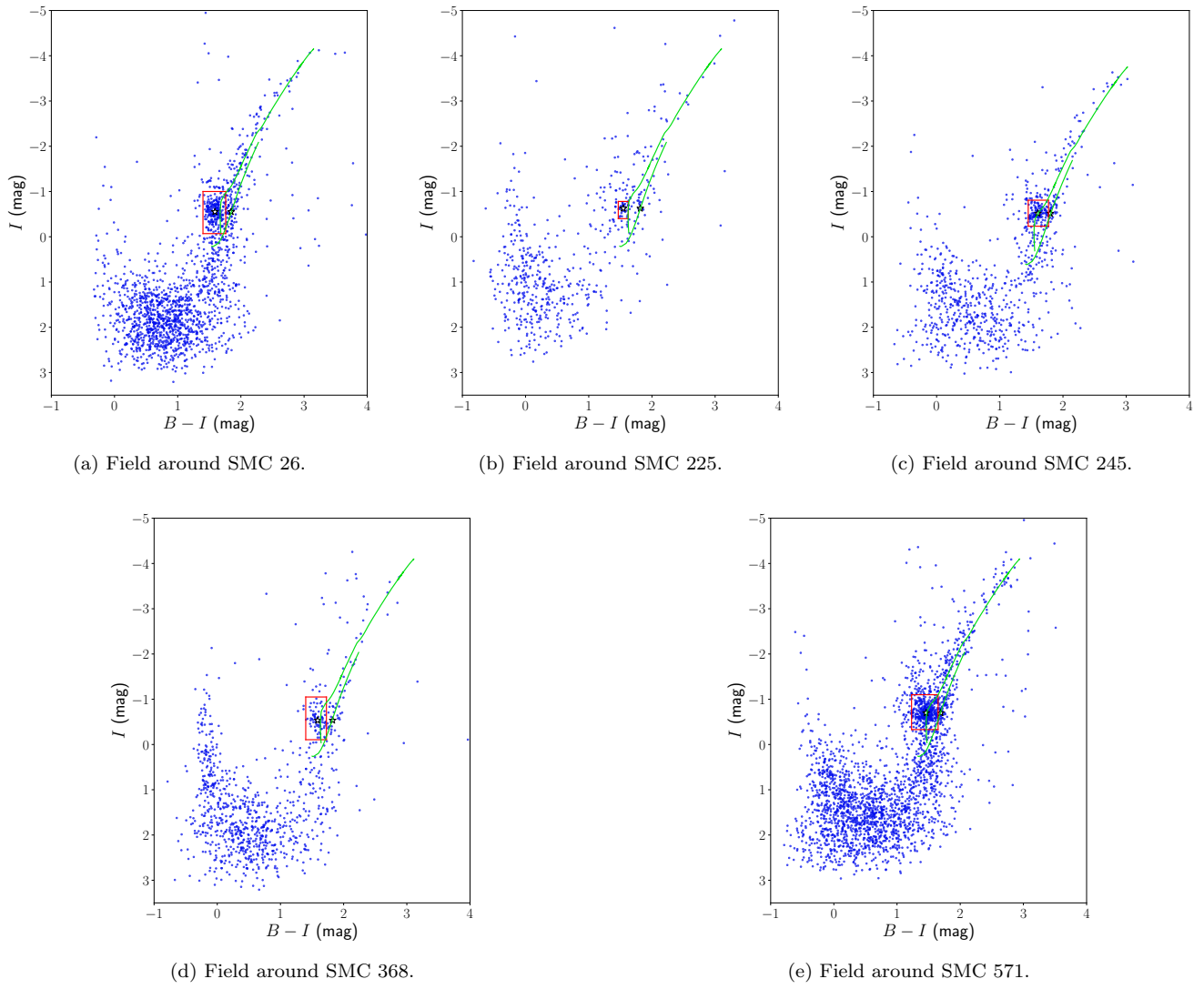


**Figure 12.** CMDs of fields surrounding clusters in the SMC. Symbols and colors are the same as in Figure 6.